Structural information from multilamellar liposomes at full hydration: Full *q*-range fitting with high quality x-ray data

Georg Pabst, Michael Rappolt, Heinz Amenitsch, and Peter Laggner*
Institute of Biophysics and X-ray Structure Research, Austrian Academy of Sciences, Steyrergasse 17, A-8010 Graz, Austria
(Received 3 November 1999; revised manuscript received 18 February 2000)

We present a method for analyzing small angle x-ray scattering data on multilamellar phospholipid bilayer systems at full hydration. The method utilizes a modified Caillé theory structure factor in combination with a Gaussian model representation of the electron density profile such that it accounts also for the diffuse scattering between Bragg peaks. Thus the method can retrieve structural information even if only a few orders of diffraction are observed. We further introduce a procedure to derive fundamental parameters, such as area per lipid, membrane thickness, and number of water molecules per lipid, directly from the electron density profile without the need of additional volumetric measurements. The theoretical apparatus is applied to experimental data on 1-palmitoyl-2-oleoyl-*sn*-glycero-3-phosphocholine, and 1,2-dipalmitoyl-*sn*-glycero-3-phosphoethanolamine liposome preparations.

PACS number(s): 87.64.Bx, 61.30.Cz, 61.10.Eq, 61.30.Eb

I. INTRODUCTION

Phospholipids are the main constituents of biological membranes that form the structural matrix into which functional membrane units such as proteins are imbedded. Among the various structures that are formed by phospholipid membranes, the lamellar liquid crystalline phase is the biologically most relevant one. Interest in the structure and physical properties of this particular phase has therefore always been an important subject in biophysical and biochemical research, since the structure is directly related to the function of the molecular aggregates. Not only do efforts to understand the function of biological membranes drive the progress in phospholipid structure research, but phospholipid-based rational drug design and biomimetic material development rely on physical interaction predictions.

The structural characterization of phospholipid model membranes was initiated by the pioneering work of Luzzati and co-workers [1,2] on unoriented multilayers of diacylphosphocholines, and was followed by a large number of x-ray and neutron scattering experiments on different phospholipid bilayer structures [3,4]. However, the major difficulties in obtaining accurate structural data arise, apart from thermal disorder (''disorder of the first kind''), from disorder in the crystal lattice (''disorder of the second kind''), which is mostly dominant in liquid crystalline phases due to their liquid properties. Two theories have been developed to model the lattice structure factor of model membranes, both accounting for deficiencies in the long range order: paracrystalline theory (PT), a general theory for disorder of the first and second kind, originated by Hosemann and Bagchi [5] and Guinier [6]; and Caillé theory (CT) [7], which was invoked for smectic liquid crystals only. The main difference between the two models is that the paracrystalline theory describes stochastic fluctuations of single, ideally flat layers, whereas Caillé theory also considers bilayer undulations by applying a Hamiltonian description derived from the free energy density of a lipid bilayer, originally derived by De Gennes [8]. In 1994 the Caillé theory was modified by Zhang, Suter, and Nagte [9] (MCT), in order to take the finite size of the lamellar stack into account; a similar expression was obtained by the authors of Ref. [10]. Both theories (PT and MCT) were applied to experimental data [10–17], but with the help of the high resolution capabilities of modern synchrotron radiation sources the superiority of the Caillé theory was clearly demonstrated [15]. The facts therefore encourage one to use the MCT for smectic-*A* liquid crystals, and moreover tests on our own data gave better fits for MCT than for PT modes (results not shown).

However having a theory that well describes the crystal lattice, and thus the position and shapes of the diffraction peaks, does not overcome a principal problem of liquid crystallography: As a consequence of lattice disorder, multilamellar liposomal suspensions hardly give rise to a sufficient number of diffraction orders to derive structural information. Among the zwitterionic phospholipids the situation is somewhat better for phosphatidylethanolamine (PE) membrane stacks, exhibiting four Bragg peaks throughout the whole L_α phase, whereas the higher water content in phosphatidylcholine (PC) bilayers leads to a higher lattice disorder and thus to even less diffraction peaks observed. As a consequence, the electron density profiles are very poor in detail, and likely to be affected by Fourier truncation errors. There are two ways to circumvent this problem, both applying osmotic pressure techniques. (1) One is to incubate multilamellar liposomes in aqueous solutions containing various concentrations of large, neutral polymers such as dextran or polyvinylpyrrolidone [14–21]. With such ''swelling experiments'' the system is partly dehydrated, and consequently the number of observed diffraction orders increases. Structural parameters for the fully hydrated bilayer are then obtained by extrapolating the areas per lipid, derived from the partly dehydrated systems to full hydration [14–17]. (2) Even more structural information can be obtained by exposing oriented multilayers to constant relative humidity atmospheres [21–25], and, depending on the degree of hydration, up to ten

*Email address: Peter.Laggner@oeaw.ac.at

diffraction orders have been recorded [23,24]. The electron density profile from such experiments is much richer in information, and even allows for a quasimolecular modeling, first applied by Wiener and White [23,26,27]. The phospholipid molecule is partitioned into quasimolecular fragments, and the contribution of each fragment to the bilayer profile is modeled by a Gaussian distribution. In this manner structural details have been obtained by a joint refinement of neutron and x-ray data sets [23]. Still, the major drawback of measuring an oriented sample in humidity chambers is that the bilayer repeat does not swell to the value reached in the unoriented case under excess water conditions, even at 100% relative humidity. Consequently, the fully hydrated L_α phase cannot be exploited with this technique. The so-called ''vapor pressure paradox'' has for a long time been a disputed topic in the lipid community. Recently, Katsaras installed a new cell for oriented bilayers [28], and demonstrated that the vapor pressure paradox originates simply from experimental inadequacy and has no theoretical background [29]. Hence the ghost of the vapor pressure paradox ceased haunting the brains of lipid scientists, and diffraction experiments on oriented membrane stacks will be of prime importance in future phospholipid structure research.

Unoriented multilamellar liposomes at full hydration are still a frequent measurement situation. Not least, simulations of biological systems and the development of new drugs, e.g., carrier systems, will always demand work with liposomal dispersions in the excess water situation. Here the information content is very low, if only Bragg peaks are considered in the data analysis. We invoke a model that also accounts for the diffuse scattering of the bilayer between diffraction peaks, and thus exploits the complete data recorded in a continuous q range. In this way our method is capable of retrieving fundamental structural parameters, such as membrane thickness, area per lipid, and number of waters, even under above conditions, when only a few orders of diffraction are observed. We further introduce a procedure, based on simple geometric relationships, to calculate the above named parameters directly from a electron density model of the bilayer, without the need of extra volumetric measurements.

II. THEORY

The intensity scattered from a finite stack of unoriented bilayers is described by

$$I(q) \propto \frac{\langle |f(q)|^2 s(q) \rangle}{q^2}, \tag{1}$$

where q is the absolute value of the scattering vector ($q = 4\pi \sin\theta/\lambda$), $f(q)$ the form factor, and $s(q)$ the structure factor. The form factor characterizes the electron density distribution, and is given in the case of a layered structure by the Fourier transform

$$f(q) = \int \rho(z) \exp(iqz)\, dz \tag{2}$$

of the electron density profile ρ along the z axis. The structure factor accounts for the crystalline or quasicrystalline nature of the lattice of the bilayer stack in the liquid crystalline phase. Both the structure and form factor are averaged over the bilayer fluctuations. By assuming that fluctuations within the bilayer are independent of fluctuations of the lattice points, the structure factor and the form factor can be treated separately according to Debye [6]:

$$I(q) \propto \frac{1}{q^2} [|\langle f(q) \rangle|^2 \langle s(q) \rangle + N(\langle |f(q)|^2 \rangle - |\langle f(q) \rangle|^2)]. \tag{3}$$

The last term in Eq. (3) gives rise to a diffuse scattering, and is usually neglected when structural information is derived from Bragg peaks only. The standard data analysis procedure is then to fit the Bragg reflections with the appropriate structure factor multiplied by a constant form factor for each single peak, which is a reasonable assumption in the vicinity of the diffraction peaks only. The electron density profile relative to the constant electron density of the buffer (water) is calculated by the Fourier synthesis

$$\rho^*(z) = \sum_{h=1}^{h_{\max}} \pm F_h \cos\left(\frac{2\pi h z}{d}\right), \tag{4}$$

wherein h is the order of reflection, and d the size of the unit cell.

We invoke a model that tries to solve the problem in the backward direction by means of an inverse Fourier transform. Since we record data in a continuous q range, we should rather model the scattering function $I(q)$ in the whole range studied. The electron density profile—at a given resolution of four diffraction orders—can be modeled according to Ref. [30] by a summation of two Gaussians, each representing the polar headgroup and the methyl terminus,[1] respectively,

$$\rho(z) = \rho_{CH_2} + \overline{\rho}_H \left[\exp\left(-\frac{(z - z_H)^2}{2\sigma_H^2} \right) + \exp\left(-\frac{(z + z_H)^2}{2\sigma_H^2} \right) \right] + \overline{\rho}_C \exp\left(-\frac{z^2}{2\sigma_C^2} \right), \tag{5}$$

where the electron densities of the headgroup $\overline{\rho}_H$ and hydrocarbon tails $\overline{\rho}_C$ are defined relative to the methylene electron density ρ_{CH_2}:

$$\overline{\rho}_H \equiv \rho_H - \rho_{CH_2}$$
$$\overline{\rho}_C \equiv \rho_C - \rho_{CH_2} \tag{6}$$

(Fig. 1). The position of the Gaussian peak is at $z_i (i = H, C; z_C = 0)$, with a standard deviation of σ_i. The form factor of this electron density model can be calculated analytically by applying Eq. (2),

[1] Wiener and White were able to model the bilayer profile with a summation of eight Gaussians [23], representing quasimolecular phospholipid fragments for oriented dioleoylphosphatidylcholine bilayers at 66% RH. However, this model is not applicable for the present case of the resolution limit of few and fewer diffraction orders.

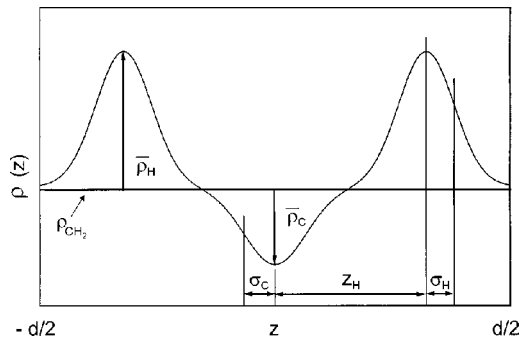

FIG. 1. Electron density profile model $\rho(z)$ as a function of distance z from the center of the bilayer, given by a summation of two Gaussians [see Eq. (5)].

$$\langle f(q)\rangle = F(q) = 2F_H(q) + F_C(q), \tag{7}$$

where the individual components denote the form factor of the headgroup

$$F_H(q) = \sqrt{2\pi}\sigma_H\overline{\rho}_H \exp\left(-\frac{\sigma_H^2 q^2}{2}\right)\cos(qz_H) \tag{8}$$

and the form factor of the hydrocarbon chains:

$$F_C(q) = \sqrt{2\pi}\sigma_C\overline{\rho}_C \exp\left(-\frac{\sigma_C^2 q^2}{2}\right). \tag{9}$$

Equation (7) gives the time averaged form factor of the bilayer as a continuous function of the scattering vector q.

Since the structure factor retained from the Caillé theory considers the lattice disorder, a full q-range description will also account for the diffuse scattering term in Eq. (3). We choose the discrete formula of the MCT structure factor [9] in the equivalent form of

$$\begin{aligned}\langle s(q)\rangle &= S(q)\\ &= N + 2\sum_{k=1}^{N-1}(N-k)\cos(kqd)\\ &\quad\times e^{-(d/2\pi)^2 q^2 \eta_1 \gamma}(\pi k)^{-(d/2\pi)^2 q^2 \eta_1},\end{aligned} \tag{10}$$

given in a paper by Lemmich *et al.* [31]. The mean number of coherent scattering bilayers in the stack is denoted as N, and γ is Eulers' constant. The Caillé parameter η_1 involves both the bending modulus K of lipid bilayers and the bulk modulus B for compression [7,9],

$$\eta_h = \frac{q^2 kT}{8\pi\sqrt{KB}}, \tag{11}$$

with

$$\eta_h = \eta_1 h^2. \tag{12}$$

However, during our data analysis we discovered an additional diffuse scattering contribution, which is not described by the MCT. Its origin is attributed to bilayers with strong lattice defects or unilamellar vesicles, which display neither short-range nor (quasi-)long-range order. The total scattered intensity is therefore given by the diffraction of the phospholipid multilayers within the quasi-long-range order lattice, plus the additional diffuse scattering of single, uncorrelated bilayers

$$I(q) \propto \frac{1}{q^2}(|F(q)|^2 S(q) + N_{\text{diff}}|F(q)|^2). \tag{13}$$

In further context of this paper we will refer to the above described model as MCG, since it is a combination of MCT and a Gaussian electron density representation of the headgroup [30].

A further benefit of this method is that one can derive structural parameters from simple geometric relationships, without the need of volumetric data as, e.g., in the approach of McIntosh and Simon [32], or Nagle *et al.* [14]. For determining the area per lipid, we follow the formalism given by Lemmich *et al.* [33] by calculating the ratio $\tilde{\rho}_r \equiv \overline{\rho_H}/\overline{\rho_C}$ [see Eq. (5)], which yields

$$A = \frac{1}{\rho_{CH_2}(\tilde{\rho}_r - 1)}\left(\frac{\tilde{\rho}_r n_C^e}{d_C} - \frac{n_H^e}{d_H}\right), \tag{14}$$

where n_C^e is the number of hydrocarbon electrons and n_H^e the number of headgroup electrons, respectively. The headgroup size d_H can be estimated from the full width at half maximum (FWHM) of the Gaussian, representing the headgroup $\sigma(\text{FWHM})_H$, and the hydrocarbon chain length d_C can be derived from

$$d_C = z_H - \frac{\sigma(\text{FWHM})_H}{2} \tag{15}$$

Further parameters of interest are the bilayer thickness

$$d_B = 2\left(z_H + \frac{\sigma(\text{FWHM})_H}{2}\right); \tag{16}$$

the thickness of the water layer,

$$d_W = d - d_B, \tag{17}$$

and the number of interbilayer free water per lipid molecule,

$$n_W^* = \frac{A d_W}{2V_W} \tag{18}$$

(see, e.g., Refs. [1,14,32]), where V_W is the volume of one water molecule (approximately 30 Å^3). The total number of water molecules including the molecules intercalated into the bilayer, can be estimated from the distance of the headgroup to the bilayer center z_H:

$$n_W = \frac{A(d/2 - z_H)}{V_W}. \tag{19}$$

Finally, the electron density profile can be set on an absolute scale. Here we follow the procedure introduced by Nagle and Wiener [34] by calculating the integral

$$A\int_0^{d/2}(\rho(z)-\rho_{CH_2})dz = A\alpha\int_0^{d/2}\left[\overline{\rho}_H\exp\left(-\frac{(z-z_H)^2}{2\sigma_H^2}\right)+\overline{\rho}_C\exp\left(-\frac{z^2}{2\sigma_C^2}\right)\right]dz, \quad (20)$$

where α is the instrumental scaling constant. The evaluation of the left integral gives

$$A\int_0^{d/2}(\rho(z)-\rho_{CH_2})dz = n_L^e + n_W^e - \frac{\rho_{CH_2}Ad}{2}, \quad (21)$$

with n_L^e being the number of electrons of the phospholipid molecule, and n_W^e the number of water electrons, i.e., the total number of waters per lipid molecule times the number of electrons in one water molecule. The integral on the right is given by

$$\begin{aligned}\Gamma &= \int_0^{d/2}\left[\overline{\rho}_H\exp\left(-\frac{(z-z_H)^2}{2\sigma_H^2}\right)+\overline{\rho}_C\exp\left(-\frac{z^2}{2\sigma_C^2}\right)\right]dz \\ &= \sqrt{\frac{\pi}{2}}\overline{\rho}_H\sigma_H\left[\operatorname{erf}\left(\frac{d/2-z_H}{\sqrt{2}\sigma_H}\right)-2\operatorname{erf}\left(\frac{a-z_H}{\sqrt{2}\sigma_H}\right)-\operatorname{erf}\left(\frac{z_H}{\sqrt{2}\sigma_H}\right)\right]+\sqrt{\frac{\pi}{2}}\overline{\rho}_C\sigma_C\left[\operatorname{erf}\left(\frac{d/2}{\sqrt{2}\sigma_C}\right)-2\operatorname{erf}\left(\frac{a}{\sqrt{2}\sigma_C}\right)\right], \quad (22)\end{aligned}$$

the parameter a is the root of the function $\rho(z)-\rho_{CH_2}$. By combining both results [Eqs. (21) and (22)], one arrives at

$$\alpha = \frac{n_L^e + n_W^e - \frac{\rho_{CH_2}Ad}{2}}{A\Gamma} \quad (23)$$

for the instrumental scaling constant. The electron density on an absolute scale is then given by

$$\rho_{\mathrm{abs}}(z) = \rho_{CH_2} + \alpha\left\{\overline{\rho}_H\left[\exp\left(-\frac{(z-z_H)^2}{2\sigma_H^2}\right)+\exp\left(-\frac{(z+z_H)^2}{2\sigma_H^2}\right)\right]+\overline{\rho}_C\exp\left(-\frac{z^2}{2\sigma_C^2}\right)\right\} \quad (24)$$

[cf. Eq. (5)].

III. EXPERIMENTAL METHODS

A. Sample preparation

1 - palmitoyl - 2 - oleoyl - *sn* - glycero - 3 - phosphocholine (POPC) and 1,2-dipalmitoyl-*sn*-glycero-3-phosphoethanolamine (DPPE) were purchased from Avanti Polar Lipids, Birmingham AL and used without further purification. Multilamellar liposomes were prepared by dispersing weighted amounts of dry lipids, typically 20–30 % w/w, in bidistilled water. To ensure complete hydration, the lipid dispersions were incubated for about 4 h at least 10 °C above the main transition temperature. During this period the lipid dispersions were vigorously vortexed. Aqueous dispersions of this lipid display narrow, cooperative melting transitions within the limits of published values, thus proving that the lipid purity corresponds to the claimed one of 99%. The POPC dispersions were further subjected to a centrifugation (centrifuge: 3K18, Sigma, Germany rotor: 12×1.5 (maximum 2.2 ml) time: 10 min 12 000 rpm) to determine the content of unilamellar vesicles [35]. The phospholipid content in the supernatant was assayed by an enzymatic kit test (Phospholipides enzymatiques PAP 150, bioMérieux, France). A proportion of 0.1–0.2 % of the total phospholipids was found as unilamellar vesicles in the supernatant. Thus, diffuse scattering from unilamellar vesicles can be neglected.

B. Experimental protocol

Small angle x-ray scattering (SAXS) experiments were carried out at the SAXS beam line, ELETTRA [36,37]. The diffraction patterns were recorded with a one-dimensional position sensitive detector [38] monitoring the q range between $2\pi/90$ and $2\pi/10$ Å^{-1} at a photon energy of 8 keV. The lipid dispersions were kept in a thin-walled 1-mm-diameter Mark capillary held in a steel cuvette, which provides good thermal contact to the Peltier heating unit. Exposure times were typically in the range of 5 min. Random thin layer chromatography tests for radiation damage resulted normal, i.e., they showed no decomposition products. The position calibration of the detector was performed by using the diffraction pattern of silver behenate powder [$CH_3(CH_2)_{20}COOAg$] (the repeat unit is 58.38 Å) [39].

C. Data analysis

The x-ray data were analyzed in terms of the model developed in Sec. II. After subtracting the background scattering from water and the sample cell, we applied the following procedure. First, the Bragg reflections were fitted by Lorentzians, taking the square root of the peak area as an estimate for the constant form factor of each peak. Utilizing Eq. (4) a raw electron density profile was calculated with the appropriate phases (− − + − −) [24,32]. The profile was then fitted with the electron density model [Eq. (5)], taking the results as input parameters for the further calculations. Thereafter, the diffraction pattern was fitted in the complete q range by operating Eqs. (7) and (10), where the finite instrumental resolution has to be accounted for by the convolution

$$I_{\mathrm{abs}}(q) = \beta\int_{-\infty}^{+\infty} I(q')r(q-q')dq', \quad (25)$$

β is the instrumental scaling constant. We chose an instrumental resolution function r with a Gaussian profile

$$r(q) = \exp\left(-\frac{q^2}{2\sigma_r^2}\right), \quad (26)$$

where the standard deviation σ_r is typically in the range of 2×10^{-4} Å^{-1} for the given experimental setup. The number

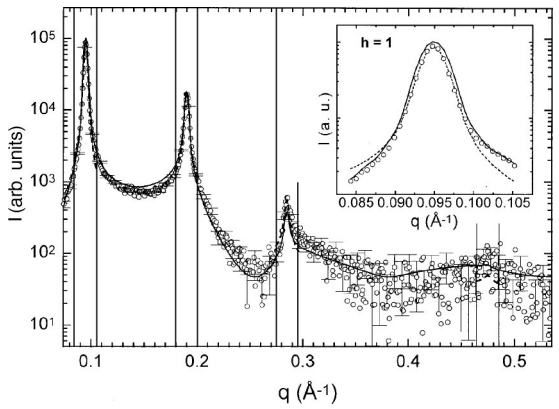

FIG. 2. The best fit of the MCG model (solid line) and MCT model (dashed line within the marked peak region) to the diffraction pattern of POPC at 2 °C. The inset gives a zoom of the first order Bragg peak.

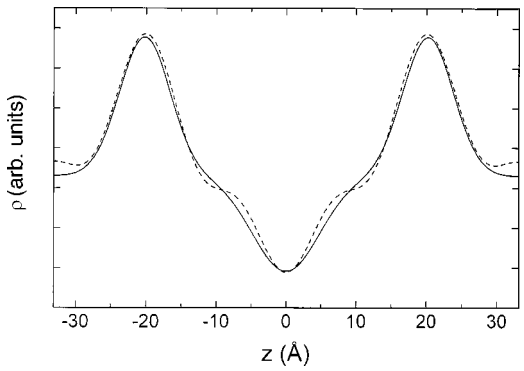

FIG. 3. Comparison of the electron density profile for POPC bilayers at 2 °C obtained by a Fourier synthesis (dashed line), using MCT and MCG refined profiles (solid line).

of fit parameters is 9 compared to 8 for the MCT model at four orders of diffraction [9]. A least square fitting was performed with self-written IDL (Interactive Data Language) procedures, utilizing MPFIT [40], which is based on the MINPACK library [41]. Structural parameters were calculated according to Eqs. (14)–(19).

IV. EXPERIMENTAL RESULTS

We measured x-ray diffraction profiles from unoriented liposomal suspensions of POPC and DPPE at 20 and 30 % w/w lipid concentrations, respectively. Both phospholipid samples were measured in the lamellar liquid crystalline phase (smectic *A*); POPC was equilibrated at 2 °C and 50 °C, and DPPE at 75 °C.

Figure 2 shows the diffraction pattern of POPC. Diffraction order numbers of 1, 2, 3, and 5 are observed; the fourth order is ruled out by the form factor. The background between the Bragg reflections is clearly modulated by the bilayer form factor, most dominantly between the first and third orders. The solid line gives the best fit of the MCG model, developed in Sec. II [Eqs. (1), (7), (10), and (25)]. The results for the fit parameters are given in the first column of Table I. Note that no diffuse background is fitted. The system is equilibrated at 2 °C only, and hence lattice defects are much more suppressed than at higher temperatures, where molecular motions are more destructive to the lattice order. Figure 2 further depicts the MCT fit (dashed line) within a q range of ± 0.01 Å^{-1} around each Bragg peak (cf. Ref. [14]); a close view of the first-order peak is drawn in the inset to Fig. 2. The comparison demonstrates two facts: First, the standard MCT uses only a small fraction of the available diffraction data. Second, the MCT gives a better fit for the peak tops, but a poorer fit for the peak tails, as it applies a constant form factor within the fitted peak region. Neither of the model functions perfectly describes the experimental data points. With the MCT method it is apparently easier to model the scattered intensity in a limited regime around the Bragg peaks, while the MCG proved to be better suited to model the asymmetric tails. A quantitative comparison of the two models in terms of the respective, reduced χ^2 sums is not expedient, as different numbers of data points are considered. It is more important to state that the MCG gives a qualitatively good fit for the full q range, i.e., the diffraction peaks including the diffuse scattering, whereas the MCT works in the vicinity of Bragg peaks only.

TABLE I. Fit results for the diffraction patterns of POPC at 2 °C and 50 °C, and DPPE at 75 °C (cf. Fig. 1). The parameters $\overline{\rho_H}$ and $\overline{\rho_C}$ are given in absolute units according to Eq. (24) (also see Fig. 6).

	POPC		DPPE
Fit parameter	$T=2$ °C	$T=50$ °C	$T=75$ °C
z_H (Å)	20.2±0.1	17.0±0.3	19.2±0.1
σ_H (Å)	3.6±0.1	3.6±0.2	3.3±0.1
$\overline{\rho_H}$ (e/Å^3)	0.11±0.01	0.11±0.01	0.15±0.01
σ_C (Å)	4.8±0.2	6.8±0.7	2.5±0.2
$\overline{\rho_C}$ (e/Å^3)	−0.08±0.01	−0.10±0.02	−0.06±0.01
d (Å)	66.2±0.1	64.3±0.1	51.4±0.1
η_1	0.0504±0.0005	0.092±0.001	0.016±0.001
N	28.0±1.0	23.0±1.0	52±1
N_{diff}	0.0	0.17±0.09	1.08±0.04

Figure 3 shows the differences between the MCT and MCG in terms of the electron density profiles. The Fourier synthesis for the MCT fit shows an anomalous, small hump at the center of the water layer, due to truncation errors. The MCG model, on the other hand, gives a smoother representation of the bilayer profile, since by definition it excludes Fourier truncation errors [Eq. (5)]. However, with four diffraction orders given, both profiles yield similar structure results. Thus full advantage of the MCG can be taken only on data with less Bragg peaks.

At 50 °C the scattered intensity of POPC exhibits different features (Fig. 4). Evidently, the number of clearly recognizable diffraction orders has decreased from 4 to 2, an effect which is attributed to stronger thermal induced fluctuations of the bilayers, but not only to this. The position of the third-order Bragg peak is close to a minimum of the bilayer form factor, therefore, the third-order is also attenuated because of the bilayer structure. Applying Fourier methods, such as the MCT, gives in this case only very rough structural information, as only two diffraction orders can be used to construct the electron density profile [cf. the inset to Fig. 4 (dashed line)]. The MCG model (solid line), on the other hand, gives a clearly refined picture of the bilayer, which

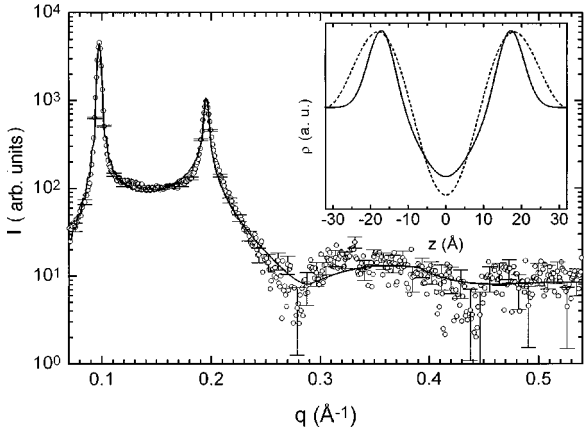

FIG. 4. The best fit of the MCG model (solid line) to the diffraction pattern of POPC at 50 °C. The inset gives the electron density profile obtained by a Fourier synthesis (dashed line), using Lorentzians to fit the Bragg peaks, and the profile refined with the MCG model (solid line).

especially affects the headgroup region, whereas the terminating methylene group remains strongly smeared. Further, one should expect a diffuse scattering from lattice defects, as the temperature has increased from 2 °C to 50 °C. Indeed, we find a diffuse contribution of the bilayer form factor (cf. Table I). An additional fingerprint for enhanced fluctuations at higher temperatures is the Caillé parameter η_1, which is almost two times greater than at 2 °C.

Compared to POPC, the diffraction pattern of DPPE (Fig. 5) exhibits a completely different characteristic, regarding both the number of observed Bragg peaks—here we detect the first four orders—as well as the diffuse background between the reflections. The solid line again gives the best fit of the MCG model. The fit is in good agreement with the experimental data, the fit results are given in Table I. Here the model also fits a contribution of diffuse scattering, which is again attributed to the enhanced molecular motions at 75 °C. The inset to Fig. 5 illustrates the effect of the MCG on Fourier artifacts. The unreal Fourier ripples of the Lorentzian model (dashed line), a consequence of the Fourier synthesis

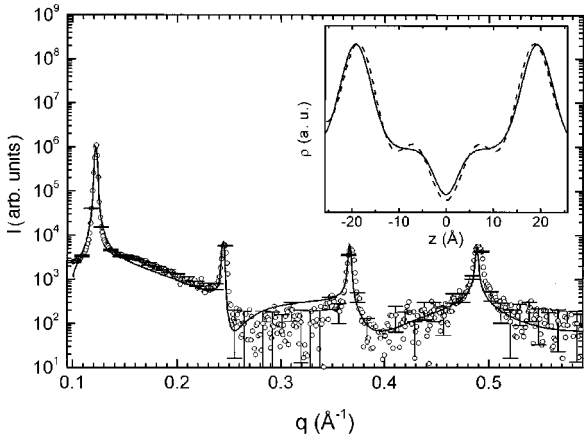

FIG. 5. The best fit of the MCG model (solid line) to the diffraction pattern of DPPE at 75 °C. The inset gives the electron density profile obtained by a Fourier synthesis (dashed line), using Lorentzians to fit the Bragg peaks, and the profile refined with the MCG model (solid line).

TABLE II. Derived structural parameters calculated by using Eqs. (14)–(19). The results for POPC at 2 °C are compared to the values obtained by using the volumetric method [16,17,32] (cf. the Appendix).

	POPC			DPPE
	$T=2$ °C		$T=50$ °C	$T=75$ °C
Parameter	Volumetric	Geometric	Geometric	Geometric
d (Å)	66.2 ± 0.1	66.2 ± 0.1	64.3 ± 0.1	51.4 ± 0.1
d_B (Å)	50.2 ± 3.6	48.9 ± 0.3	42.5 ± 1.1	46.2 ± 0.4
d_W (Å)	16.0 ± 3.7	17.3 ± 0.4	21.7 ± 1.2	5.3 ± 0.5
d_C (Å)	16.1 ± 0.6	16.0 ± 0.2	12.8 ± 0.6	15.4 ± 0.2
A (Å^2)	56 ± 2	54 ± 1	62 ± 1	52 ± 1
n_W	22 ± 2	24 ± 1	31 ± 1	11.3 ± 0.3
n_W^*	15 ± 4	16 ± 1	23 ± 2	4.6 ± 0.4

with four terms only, are suppressed resulting in a smooth bilayer profile (solid line) that corresponds to the resolution of the experiment.

Further structural parameters have been calculated according to the geometric considerations expressed in Eqs. (14)–(19). The number of headgroup electrons is 164, and the number of hydrocarbon chain electrons is 256 for POPC, and $n_H^e=140$ and $n_C^e=242$ for DPPE. The methylene electron density is $0.317\pm0.003e/\text{Å}^3$ according to Ref. [30]. The results for the two measured samples are listed in Table II. The structural parameters of POPC at 2 °C are compared to the values obtained by the volumetric method, which was introduced by McIntosh and Simon [32,42] for phospatidylethanolamines, and further adopted for lecithins by Nagle *et al.* [14]. A brief description of the formalism is given in the Appendix. For the lipid volume, which is an input parameter of the method, we refer to the measurement of Hianik *et al.* [43], and extrapolate to 2 °C, so that we obtain $V_L^l=1223\,\text{Å}^3$. Within measurement errors, which are larger for the volumetric method, mostly due to uncertainties in the headgroup thickness [12,13] both methods result in the same values for the structural parameters (cf. columns 1 and 2 of Table II). At 50 °C, the repeat distance is reduced by 2 Å, and the bilayer thickness is increased by approximately 6 Å. On the other hand, the interbilayer water thickness is increased by roughly 4 Å, a sign for water uptake from the excess phase as observed in the increase of parameters n_W or n_W^*, respectively, due to reduced van der Walls interactions between opposing bilayers [44] at stronger undulations [45]. A further parameter which increases with temperature is the area per lipid. The structural results for DPPE give a very thin water layer of 11 water molecules per lipid molecule, out of which approximately six are intercalated into the bilayer. These values are in good agreement with the data published by McIntosh and Simon for dilauroylphosphatidylethanolamine [32]. The small fluid space in PE bilayers could arise from interbilayer hydrogen bond formation through the water molecules or electrostatic interactions between the amine and phosphate groups of opposing bilayers [32].

Finally, the electron density profiles were put on an absolute scale by applying Eqs. (20)–(24). An input parameter is the total number of electrons per lipid molecule, which is 420 for POPC and 382 for DPPE. The results are plotted in

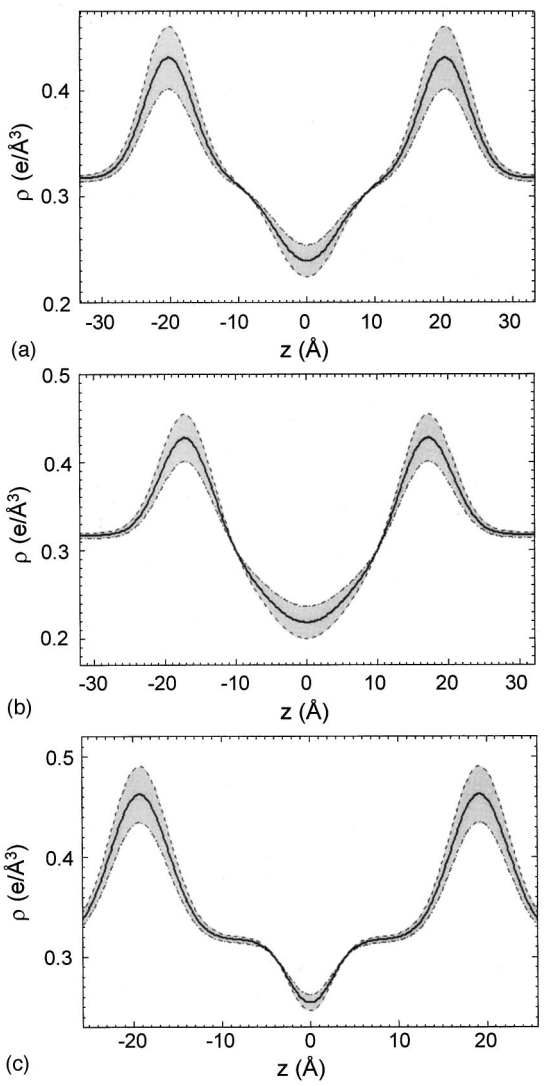

FIG. 6. Absolute electron density profiles of POPC at 2 °C (a), POPC at 50 °C (b), and DPPE at 75 °C (c). Deviations due to the error of the instrumental scaling factor α are depicted as a gray area enveloped by the maximal positive (dashed line) and negative (dot-dashed line) divergences.

Fig. 6; Figs. 6(a) and 6(b) give the absolute electron density of POPC at 2 °C and 50 °C, respectively, whereas Fig. 6(c) depicts the absolute electron density of DPPE at 75 °C.

V. DISCUSSION

A model has been introduced to analyze small angle diffraction data of unoriented phospholipid membrane stacks at high instrumental resolution. The formalism combines a form factor, related to a Gaussian representation of the electron density profile (Fig. 1), with a MCT structure factor. The proposed electron density model gives the mean structure of a phospholipid bilayer time averaged over all fluctuations, and is well suited to represent the x-ray picture one sees from not more than five orders of diffraction. Higher orders—which can be obtained by aligning the layers only—would result in a more detailed electron density profile for which another electron density model, like, e.g., hybrid types of Gaussians and strip models [34], would give a better representation. Such models have also been tried out on our data, but failed because of too many correlating fit parameters for the given instrumental resolution. It is reasonable to model the electron density profile by means of analytic functions, as the features of its structure are well known since the pioneering work of Luzzati and co-workers [1,2]. The difference in the distinct phospholipid bilayer structures are then accounted for by adjusting the parameters, i.e., headgroup position, headgroup width, etc., of the analytical function. The inverse Fourier method, which takes the form factor of the bilayer model and fits it together with a structure factor to the scattered intensity has further the advantage of excluding Fourier truncation errors. The MCG model was tested experimentally on POPC and DPPE multilayers, giving good fit results (see Sec. IV, Fig. 2, Fig. 4, Fig. 5, and Table I).

Several other models were already used [5,6,9,10,33] to perform the same task. We shall briefly discuss the most prominent ones. In 1994, Zhang and co-workers introduced the modified Caillé theory, and gave an experimental proof of its superiority to the classical paracrystalline theory [9,15]. The group usually recorded high-resolution data at a synchrotron beam line by means of a diffractometer, but in the vicinity of the Bragg reflections only. Electron density profiles were computed by applying a standard Fourier synthesis [Eq. (4)]. Conversely, we use an equivalently brilliant source, but a detecting system, which is able to monitor the diffraction pattern in a continuous range of scattering angles. In this case, applying the standard MCT data analysis, which works only in a regime close to diffraction peaks, means rejecting all the information hidden in the diffuse background scattering between the Bragg peaks (Fig. 2). This information becomes even more valuable if less than four orders are observed. Nagle and co-workers reported only two diffraction orders for unoriented dipalmitoylphosphatidylcholine, egg phosphatidylcholine, dimyristolphosphatidylcholine, and dioleoylphosphatidylcholine bilayers in excess water [14–17], which is insufficient to obtain satisfactory structural information, if only the Bragg peaks are considered. The common ways to circumvent this problem are osmotic stress experiments [14–21,23,24], where the system is partly dehydrated, and thus more diffraction orders are detected as bilayers are consequently hindered in undulation. Structural information of the fully hydrated phase is accessible then only through a numerical extrapolation to zero osmotic pressure. It is well known that extrapolations are always inherent to large uncertainties, and should be avoided if possible. The MCG model, on the other hand, also describes the diffuse scattering, and is thus capable of obtaining structural information even at low Bragg reflection information content, e.g., POPC at 50 °C (Fig. 4). Moreover, the assumption of a constant form factor for each Bragg peak is not very accurate for higher diffracting orders, as peaks broaden strongly and more and more scattered intensity is smeared to the peak tails. For instance, the third-order peak of the 2 °C POPC diffraction pattern displays an asymmetric shape (Fig. 2), which is obviously due to the modulation by a nonconstant bilayer form factor. Such effects are not seen in the x-ray data published by Zhang and co-workers, because the observation of asymmetric peak shapes is likely to depend on the lipid type and on its specific form factor, e.g., the diffraction pattern of DPPE does not exhibit any asymmetric peaks (Fig. 4). Further, data treated with the MCT

only have not always been presented in a uniform fashion, i.e., increasing the order ($h=1$ to 3) decreases the data point density [16,17] or the selected q range [15]. Thus peak asymmetries, even if present, are difficult to be seen.

The authors of Ref. [10] suggested a model similar to the MCT [9] to analyze small angle scattering data on bis 2-ethylhexyl sodium sulphosuccinate (AOT)-water systems and didodecyl dimethyl ammonium bromide (DDAB)-water systems. They combined the structure factor with the form factor of a strip model for a continuous q-range fit function. Although the strip model for the AOT-water and DDAB-water systems differs somewhat from a reasonable strip model for phospholipid bilayers, this method could in principle easily be adopted with the advantage of fewer fit parameters. Still we refer to the common criticism on strip models, which is that discontinuous boundaries between the different regions of the bilayers give an unrealistic picture of a fluctuating bilayer.

A quite different approach was introduced by Lemmich *et al.* [33] for neutron scattering experiments. They proposed a strip model for the bilayer, but averaged its form factor together with a paracrystalline structure factor without decoupling the two entities as the two other theories do [Eqs. (1) and (3)]. Lemmich *et al.* analyzed their data in terms of both their model and the MCT, but the fits gave equally good results for phospholipids in the lamellar liquid crystalline phase. The most convincing explanation is that strong instrumental smearing, inherent to neutron scattering experiments, does not allow for any decision. Since not even Lemmich *et al.* could show better fit results for phospholipids in the L_α phase, we see no argument to apply their model that would imply a recalculation of the whole formalism, since x rays ''see'' a different contrast than neutrons do.

In conclusion, we should state that the models that have been discussed are without any doubt appropriate for the measurement methods applied by the individual groups. This is clearly demonstrated by the good fits to their experimental data. However, for the given reasons our method is best tailored to extract as much information as possible from high resolution x-ray data recorded in a continuous range.

A further benefit of the MCG is that structural parameters like bilayer thickness, area per lipid, water distribution, etc., can be estimated from simple geometric considerations. Despite the gravimetric method of Luzzati [1], the commonly used method, initiated by McIntosh and Simon [32,42] and applied by Nagle *et al.* [14], relies on additional information about the lipid volume, which is supplied by specific volumetric measurements. The algorithm is built upon a comparison with a known gel phase structure, assuming that the volume of the headgroup is the same for both phases [cf. the Appendix, Eqs. (A1) and (A2)]. For phospholipids with a PC headgroup, one usually employs the structural data of DPPC in the L_β phase, published by Sun *et al.* [46,47]. A further structural input, i.e., the headgroup thickness, is needed to calculate the bilayer thickness according to the steric definition [42] [Eq. (A4)]. McIntosh and Simon suggested a value of 10 Å for PC headgroups and 8 Å for PE's, derived from space filling molecular models. The headgroup conformation of DPPC was measured by Büldt and co-workers [48,49] by means of neutron diffraction and deuteron labels, but at very low water content (10 and 25 % w/w). From the published data the heagroup thickness can be extracted as $d_H=9 \pm 1.2$ Å, a value employed by Nagle and co-workers, without considering the measurement error within which the values given by McIntosh and Büldt are equal. However, the headgroup conformation is likely to depend on temperature, pressure, chain tilt [30], or hydration [24], which directly affects the headgroup dimensions, so that the volume of the PC headgroup in the $L_{\beta'}$ phase is not evidently the same as in the L_α phase. Hence a method which utilizes the assumption of a constant headgroup volume and size, respectively, and even relies on measurements of systems different from the situation of fully hydrated bilayers, can be justifiable, but certainly leads to a rough estimate. A way out of this dilemma should be structural data from highly aligned multilayers at full hydration according to the method of Katsaras [28]. However, it is also possible to obtain reasonable estimates for unoriented systems without the need of extra data input by the simple geometric relationships of the Gaussian electron density model [Eqs. (14)–(19)]. The results compare well to those obtained by the volumetric method (cf. Table II), and even display smaller errors.

The Gaussian electron density profile can be set on an absolute scale, which is often desirable. The scaling factor is computed by integrating the profile from the center to the border of the unit cell [Eq. (20)]. This can be easily done, since the electron density profile is given as an analytic function. However, we argue to take absolute electron densities with great care, since the relative error of the scaling factor is large (0.2 for POPC at 50 °C), a consequence of the large number of error contributors in the calculation procedure. This also applies to absolute electron densities published by other groups [14–17,30], but has not been discussed there.

In conclusion, we remark that the MCC model gives considerably more structural information than the standard MCT model, provided that the number of recorded diffraction orders is less than 4. At four orders of diffraction one obtains equally good results (Fig. 3). The advantages of the model are due to a cancellation of Fourier artifacts, and a simple method to derive structural parameters. Since the model can retrieve structural information from diffuse scattering, its potential increases in importance, when less than four orders of diffraction are recorded (Fig. 4). This is a common situation for fully hydrated phosphaditylcholine bilayers, which include about three times more interbilayer water than phosphaditylethanolamine bilayer systems.

ACKNOWLEDGMENTS

The authors are grateful to J. F. Nagle and H. I. Petrache, for helpful discussions and for providing us the source code of the program MCT. We also express our thanks to F. Nallet and J. Lemmich for sending additional manuscripts, and to H. Sormann for helpful discussions on statistics. This work was supported by the ''Elettra-Project'' of the Austrian Academy of Sciences. M.R. is the recipient of a long-term grant from the European Commission under the program ''Training and Mobility of Researchers'' [Contract No. SMT4-CT97-9024(DG12-CZJU)].

APPENDIX

Structural parameters for bilayers in the lamellar liquid crystalline phase can be derived upon the assumption that the

volume of the phospholipid headgroup is equal to the volume in the gel phase [14]

$$V_H^l = V_H^g, \tag{A1}$$

where the superscript l denotes the liquid phase, and g the gel phase. By calculating the difference in the total lipid volume $V_L^l - V_L^g$, one arrives at

$$A^l = \frac{V_L^l - V_H^g}{d_C^g + \dfrac{d_{HH}^l - d_{HH}^g}{2}}. \tag{A2}$$

for the area of the fluid bilayer, where d_C is the hydrocarbon chain length and d_{HH} the head-to head-group distance over the bilayer. For phospholipids with a PC headgroup, one usually employs the structural data of L_β DPPC as published by Sun *et al.* [46]: $V_H^g = 319 \pm 6$ Å and $d_C^g = 17.3 \pm 0.2$ Å, and the corrected value of the head-to-head-group distance [47] $d_{HH}^g = 42.8 \pm 0.2$ Å. The hydrocarbon chain length is given by

$$d_C^l = \frac{V_L^l - V_H^g}{A^l} \tag{A3}$$

and the bilayer thickness, according to the steric definition of McIntosh and Simon [42], by

$$d_B^l = 2(d_C^l + d_H). \tag{A4}$$

The headgroup thickness d_H has been estimated from space filling models to be 10 Å for PC's and 8 Å for PE's, whereas Büldt and co-workers found a value of 9 ± 1.2 Å with neutron diffraction experiments at a hydration of 10% w/w [48,49]. The interbilayer water thickness and the number of free water is given according to Eqs. (17) and (18).

Sometimes it is desirable to compare the structural results with already published data derived by applying the gravimetric method of Luzzati [1]. The Luzzati bilayer thickness is calculated as

$$d_B^{\text{Luzzati}} = \frac{2V_L}{A}, \tag{A5}$$

where the corresponding interbilayer water thickness and the total number of water molecules per lipid are obtained according to Eq. (19).

[1] V. Luzzati, in *Biological Membranes*, edited by D. Chapman (Academic, London, 1967), p. 71.
[2] A. Tardieu, V. Luzzati, and F. C. Reman, J. Mol. Biol. **75**, 711 (1973).
[3] S. H. White and M. C. Wiener, in *Permeability and Stability of Lipid Bilayers*, edited by E. A. Disalvo and S. A. Simon (CRC Press, Boca Raton, FL, 1995), p. 1.
[4] S. H. White and M. C. Wiener, in *Membrane Structure and Dynamics*, edited by K. M. Merz and B. Roux (Birkhäuser, Boston, 1996), p. 127.
[5] R. Hosemann and S. N. Bagchi, *Direct Analysis of Diffraction by Matter* (North-Holland, Amsterdam, 1962).
[6] A. Guinier, *X-Ray Diffraction* (Freeman, San Francisco, 1963)
[7] A. Caillé, C. R. Seances Acad. Sci., Ser. B **274**, 891 (1972).
[8] P. G. De Gennes, J. Phys. (Paris), Colloq. **30**, C4-65 (1969).
[9] R. Zhang, R. M. Suter, and J. F. Nagle, Phys. Rev. E **50**, 5047 (1994).
[10] F. Nallet, R. Laversanne, and D. Roux, J. Phys. II **3**, 487 (1993).
[11] A. E. Blaurock and J. C. Nelander, J. Mol. Biol. **103**, 421 (1976).
[12] J. Torbet and M. H. Wilkins, J. Theor. Biol. **62**, 447 (1976).
[13] C. R. Worthington, Photochem. Photobiol. **3**, 43 (1989).
[14] J. F. Nagle *et al.*, Biophys. J. **70**, 1419 (1996).
[15] R. Zhang *et al.*, Biophys. J. **70**, 369 (1996).
[16] S. Tristram-Nagle, H. I. Petrache, and J. F. Nagle, Biophys. J. **75**, 917 (1998).
[17] H. I. Petrache, S. Tristram-Nagle, and J. F. Nagle, Chem. Phys. Lipids **95**, 83 (1998).
[18] T. J. McIntosh and S. A. Simon, Annu. Rev. Biophys. Biomol. Struct. **23**, 27 (1994).
[19] D. M. LeNeveu, R. P. Rand, and V. A. Parsegian, Nature (London) **259**, 601 (1976).
[20] D. M. LeNeveu, R. P. Rand, V. A. Parsegian, and D. Gingell, Biophys. J. **18**, 209 (1977).
[21] V. A. Parsegian, N. Fuller, and R. P. Rand, Proc. Natl. Acad. Sci. USA **76**, 2750 (1979).
[22] Y. Inoko and T. Mitsuim, J. Phys. Soc. Jpn **44**, 1918 (1978).
[23] M. C. Wiener and S. H. White, Biophys. J. **61**, 434 (1992).
[24] J. Katsaras, K. R. Jeffrey, D. S.-C. Yang, and R. M. Epand, Biochemistry **32**, 10 700 (1993).
[25] T. J. McIntosh and A. D. Magid, in *Phospholipid Handbook*, edited by G. Cevc (Dekker, New York, 1993), p. 553.
[26] M. C. Wiener and S. H. White, Biophys. J. **59**, 162 (1991).
[27] M. C. Wiener and S. H. White, Biophys. J. **59**, 174 (1991).
[28] J. Katsaras, Biophys. J. **75**, 2157 (1998).
[29] J. F. Nagle and J. Katsaras, Phys. Rev. E **59**, 7018 (1999).
[30] M. C. Wiener, R. M. Suter, and J. F. Nagle, Biophys. J. **55**, 315 (1989).
[31] J. Lemmich *et al.* (unpublished).
[32] T. J. McIntosh and S. A. Simon, Biochemistry **25**, 4948 (1986).
[33] J. Lemmich *et al.*, Phys. Rev. E **53**, 5169 (1996).
[34] J. F. Nagle and M. C. Wiener, Biophys. J. **55**, 309 (1989).
[35] K. Lohner *et al.*, Biochemistry **38**, 16514 (1999).
[36] H. Amenitsch, S. Bernstorff, and P. Laggner, Rev. Sci. Instrum. **66**, 1624 (1995).
[37] H. Amenitsch, *et al.*, J. Appl. Crystallogr. **30**, 872 (1997).
[38] A. Gabriel, Rev. Sci. Instrum. **48**, 1303 (1977).
[39] T. C. Huang, H. Toraya, T. N. Blanton, and Y. Wu, J. Appl. Crystallogr. **26**, 180 (1993).
[40] C. Markwardt, documentation for MPFIT, Internet site: http://cow.physics.wisc.edu/~craigm/idl/idl.html
[41] B. S. Garbow, K. E. Hillstrom, and J. J. Moore, documentation for MINPACK, Internet site: http://www.zrz.tu-berlin.de/~zrz/software/numerik/minpack

[42] T. J. McIntosh and S. A. Simon, Biochemistry **25**, 4058 (1986).
[43] T. Hianik *et al.*, Colloids Surf., A **139**, 189 (1998).
[44] J. Israelachvili, *Intermolecular & Surface Forces* (Academic, New York, 1991), p. 395.
[45] W. Helfrich, Z. Naturforsch., **33A**, 305 (1978).
[46] W.-J. Sun *et al.*, Phys. Rev. E **49**, 4665 (1994).
[47] W.-J. Sun *et al.*, Biophys. J. **71**, 885 (1996).
[48] G. Büldt, H. U. Gally, J. Seelig, and G. Zaccai, J. Mol. Biol. **134**, 673 (1979).
[49] G. Zaccai, G. Büldt, A. Seelig, and J. Seelig, J. Mol. Biol. **134**, 693 (1979).